

Mechanics of Crystalline Nanowires

Harold S. Park, Wei Cai, Horacio D. Espinosa, and Hanchen Huang

Abstract

Nanowires are among the most exciting one-dimensional nanomaterials because of their unique properties, which result primarily from their chemical composition and large surface area to volume ratio. These properties make them ideal building blocks for the development of next generation electronics, opto-electronics, and sensor systems. In this article, we focus on the unique mechanical properties of nanowires, which emerge from surface atoms having different electron densities and fewer bonding neighbors than atoms lying within the nanowire bulk. In this respect, atomistic simulations have revealed a plethora of novel surface-driven mechanical behavior and properties, including both increases and decreases in elastic stiffness, phase transformations, shape memory, and pseudoelastic effects. This article reviews such atomistic simulations, as well as experimental data of these phenomena, while assessing future challenges and directions.

Introduction

Over the past decade, nanowires have drawn considerable attention from the scientific community because of their remarkable physical properties.¹ These properties also have created an immense interest in using nanowires as the basic building blocks for future nanoelectromechanical systems (NEMS).² Figure 1 illustrates why nanowires can have physical properties that differ greatly from those encountered in their bulk counterpart, namely their large surface area to volume ratio. This fact is critical because surface atoms have fewer bonding neighbors, or a lower coordination number, than do bulk atoms.³ Surface atoms also differ from bulk atoms in that they are subject to surface stress that is caused by their coordination number deficiency, which can be written as^{4,5}

$$\tau = \tau^0 + S\epsilon, \quad (1)$$

where τ is the surface stress, τ^0 is the residual (strain-independent) portion of the surface stress, S is the surface elastic stiffness, and ϵ is the strain. Note that $S\epsilon$ is the surface elastic (strain-dependent) part of the surface stress.

The surface stress τ is typically tensile for fcc metals,⁶ which means the surface could lower its energy by contracting, as seen in Figure 1. The contraction allows the surface atoms to increase their coordination number and also their electron density, thereby making their bonding environment more bulk like.⁷ In contrast, semiconductor surfaces tend to reconstruct,^{8,9} or form repetitive patterns in which the surface atoms displace significantly from their initial positions, with the surface atoms also contracting toward the bulk; however, semiconductor surface stresses are typically compressive, leading in general to an increase in length for semiconductor nanowires at equilibrium.^{10–12} It is critical to note that many of the novel elastic and inelastic phenomena of nanowires that we will review result directly from the deformation and surface reconstructions caused by surface stresses.

In this article, we review recent atomistic modeling research performed using *ab initio* calculations,^{7,13} classical molecular dynamics (MD),¹⁴ and emerging simulation techniques that aim to circumvent the time scale limitations of MD.¹⁵ Such modeling has elucidated how surface effects

impact the elastic and inelastic mechanical properties of crystalline nanowires. Whenever possible, we place the atomistic modeling results in the context of available experimental data to demonstrate the current strengths, limitations, and eventual interdependencies of each field in the study of nanowire mechanics.

Surface Effects on the Elastic Properties of Nanowires

fcc Metal Nanowires

As summarized in Figure 2, there has been both scatter and overlap between the experimental measurements of metal nanowire elastic properties^{16–20} and the stiffening or softening mechanisms elucidated computationally.^{7,21–25} Note that the nanowire diameter is generally less than 10 nm for the MD simulations because the number of atoms in thicker nanowires makes it computationally prohibitive to perform MD simulations. For example, dramatic increases in the Young's modulus of $\langle 110 \rangle$ silver nanowires were found as the wire diameter decreases from 150 to 20 nm;^{18,19} atomic force microscope (AFM)-based resonance and bending were employed in these studies. Liang et al.²¹ identified a possible mechanism for the observed nanowire stiffening for copper nanowires using embedded atom method (EAM) potentials. In particular, they found that the axial compressive strain caused by surface stresses (as in Figure 1) is large enough to induce a non-linear elastic increase in the stiffness of

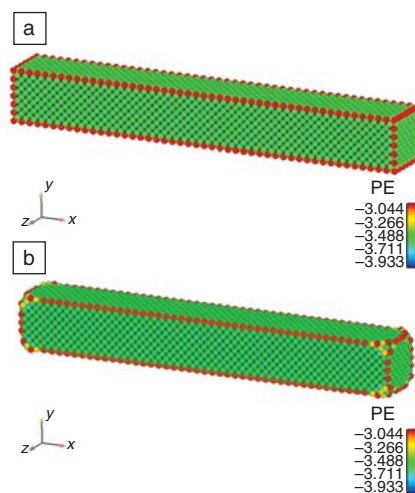


Figure 1. A 16 nm \times 2 nm \times 2 nm gold nanowire modeled using an embedded atom method potential, with individual atoms colored by their potential energy (PE). (a) Initial nanowire configuration. (b) Final, energy-minimizing configuration after 5% compressive elastic strain due to surface stresses.

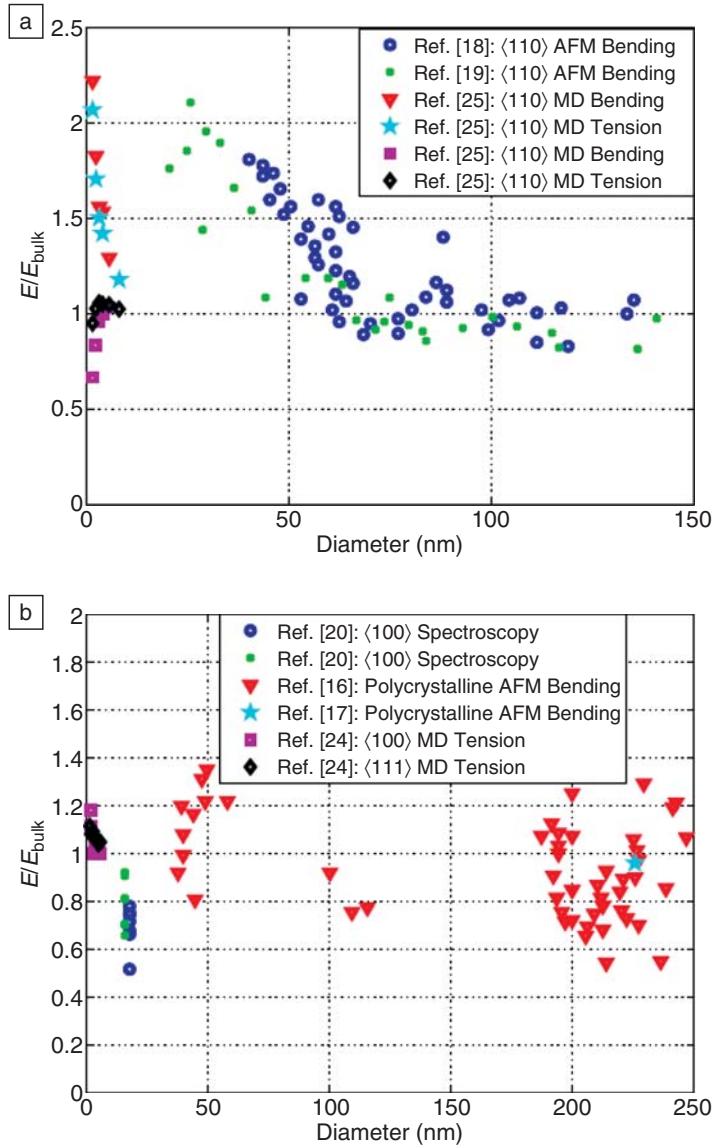


Figure 2. Normalized experimental atomic force microscopy (AFM) and computational molecular dynamics (MD) results for the size-dependent Young's modulus of (a) Ag nanowires and (b) Au nanowires.

$\langle 110 \rangle$ bulk atoms, leading to an increase in the nanowire Young's modulus.

In contrast, resonance experiments performed by Petrova et al.²⁰ on $\langle 100 \rangle$ gold nanowires revealed a decrease in Young's modulus with decreasing size (see spectroscopic analyses in Figure 2b). This finding is supported by both atomistic tension²¹ and multiscale resonance²⁶ simulations not only because $\langle 100 \rangle$ bulk atoms *soften* elastically under surface stress-induced compressive strain,^{21,26} but also because of the surface bond saturation mechanism advanced by Zhou and Huang.⁷ Using both atomistic simulations with EAM potentials and *ab initio* calculations, Zhou and Huang found that softening along the

$\langle 100 \rangle$ direction of the $\{100\}$ surface is due to coordination number reduction, which offsets any gain in surface bond strength due to increases in local electron density. In general, whether a surface is softer or stiffer than the bulk depends on whether the stiffening that is gained from electron redistribution at the surface is able to overcome the softening due to the loss of bonding neighbors. These findings indicate the reduction in Young's modulus for $\langle 100 \rangle$ nanowires occurs because of both bulk and surface softening.

Although these similarities are encouraging, most atomistic studies have determined the elastic properties of nanowires through tensile loading and have there-

fore neglected the experimentally relevant point that different loading methods (tension, bending, or resonance) may yield different elastic properties of nanowires. Resonance involves exciting the nanowire into vibrating at specific resonance frequencies, which are dependent on the geometry, stiffness, and density of the nanowire. For example, differences may emerge in nanoscale tension and bending (resonance) tests because the surfaces of the nanowire carry the most stress during flexural motion. This hypothesis has been confirmed by the atomistic studies of McDowell et al.,²⁵ as seen in Figure 2a, and Miller and Shenoy.²³ Both studies found differences in nanowire elastic properties under bending and tension. In particular, the surface effect during bending was found to be six times that under tension.²³

Semiconducting Nanowires

The elastic properties of semiconducting nanowires, as measured experimentally^{10,27-38} and predicted computationally,^{11,39-42} also exhibit both scatter and overlap, as seen in Figure 3. However, the mechanisms causing the scatter and variations from bulk properties have been further elucidated by direct comparison between MD simulation and electron microscopy tests.^{10,43} These studies directly coupled, for the first time, experimental tensile tests on 20–400 nm $[0001]$ ZnO nanowires⁴⁴⁻⁴⁶ with MD simulations of tensile loaded 5–20 nm ZnO nanowires. The combined results, reported in Figure 3a, show that Young's modulus increases from 140 GPa (bulk value) to 194 GPa as the wire size decreases from 80 to 5 nm; other experiments on $[0001]$ ZnO nanowires also have predicted a similar stiffening with decreasing size,^{35,36} as seen in Figure 3a.

The MD simulations by Agrawal et al.¹⁰ predicted elastic stiffening in ZnO nanowires arising from a decrease in surface interatomic spacing due to surface reconstruction. This is in agreement with a previous hypothesis based on experimental data fitting³⁵ but differing from the mechanism of bulk nonlinear elasticity found by other researchers using MD.^{39,41} In contrast, *ab initio* calculations⁴² reveal much smaller surface bond strains, suggesting that surface bond saturation resulting from an increased electron density, and not bulk nonlinear elastic effects, may be responsible for the increase in Young's modulus with decreasing nanowire size. These results highlight the limitations of classical interatomic potentials in capturing the underlying electronic effects that drive surface reconstructions.

A decrease in the Young's modulus of $\langle 110 \rangle$ silicon nanowires was measured

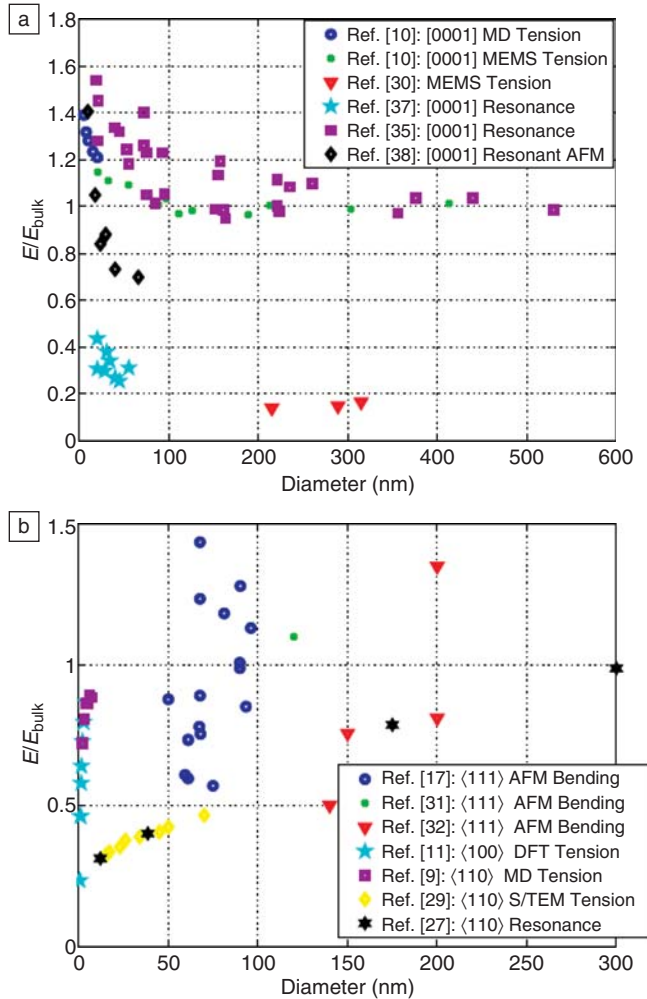


Figure 3. Normalized experimental (microelectromechanical system [MEMS], atomic force microscope [AFM], (scanning) transmission electron microscope [(S)TEM], resonance), and computational (molecular dynamics [MD], density functional theory [DFT]) results for the size-dependent Young's modulus of (a) ZnO nanowires and (b) Si nanowires.

experimentally for sub-100 nm nanowire diameters.^{27–29} Lee and Rudd¹¹ captured the softening effect using density functional theory (DFT) calculations of hydrogen passivated $\langle 100 \rangle$ silicon nanowires. However, the Young's modulus was found to approach the bulk value for nanowire diameters larger than 4 nm. They also found that nonlinear bulk elasticity has a negligible effect on the Young's modulus of silicon nanowires. It should be noted that the hydrogen passivation of the silicon surfaces in the DFT calculations mitigates the surface stress of reconstructed surfaces by increasing the coordination number of the surface atoms.

To investigate this effect, Kang and Cai^{9,12} modeled $\langle 110 \rangle$ silicon nanowires using the modified EAM (MEAM) potential, in which surface reconstruction occurs without hydrogen passivation.

Interestingly, the MEAM potential predicted surface reconstructions with patterns similar to those predicted by DFT. The MEAM model also predicted a bulk Young's modulus for nanowire diameters larger than 4 nm. Shim et al.⁸ also considered the effects of surface reconstructions and found that bond saturation, and therefore the surface stiffness, is strongly influenced by the nature of the surface reconstruction. Again, these atomistic studies focused on tensile loading; multi-scale resonance calculations by Park⁴⁷ predicted elastic softening in $\langle 100 \rangle$ silicon nanowires when the wire diameter dropped below 30 nm.

The preceding discussion makes clear that a substantial gap exists between computational predictions and experimental measurements of the Young's modulus of both metallic and semicon-

ducting nanowires. In particular, Figures 2 and 3 highlight a key discrepancy: experimental predictions of the nanowire Young's modulus deviate from the bulk Young's modulus at diameters smaller than about 100 nm. This diameter is considerably larger than the transition diameter predicted by MD simulations, where deviations from the bulk are not observed for wire diameters larger than approximately 10 nm.

Closing the gap between experiment and MD simulation will require resolution of the following issues: (1) identifying dominant atomistic mechanisms, either known (surface bond saturation, reconstructions, nonlinear bulk elasticity) or unknown, in the various loading modes that are commonly utilized experimentally (bending,^{16,17,19,31,32} resonance,^{18,20,27,33,35,36,48} tension^{10,28–30}); (2) accounting for the fact that experimentally synthesized nanowires are not defect-free (e.g., native oxide layers, pre-existing defect patterns, polycrystalline texture) in contrast to the perfect single crystal nanowires studied using atomistic simulation; (3) eliminating experimental uncertainty in instrument calibration, fixing and mounting of samples, measurement of nanowire diameter or cross-sectional area, and boundary and loading conditions.¹⁰

Surface Effects on the Inelastic Behavior and Properties of Nanowires

Nanowire Plasticity

There has been considerable research using atomistic simulations to study, mainly via axial tension and compression, the inelastic behavior and properties of crystalline nanowires.^{9,14,39,49–68} One key finding is that nanowires exhibit different failure modes, which leads to disparate strengths in tension and compression. Diao et al.^{14,50,69} found that $\langle 100 \rangle / \langle 100 \rangle$ gold nanowires yield via nucleation and propagation of both full and partial dislocations under tensile loading, whereas only partial dislocations are observed in compressive loading. Experimentally, Marszalek et al.,⁷⁰ using scanning probe microscopy, directly measured displacements corresponding to stacking fault generation on $\{111\}$ crystal planes during tensile loading of sub-2 nm gold nanowires; such stacking faults have been observed in nearly all MD simulations of fcc metal nanowire plasticity.

Rodrigues et al.^{61,71} showed experimentally using high resolution transmission electron microscopy (TEM) that changing the axial orientation of sub-3 nm gold nanowires changes the modes of plasticity

and failure. MD simulations have elucidated the mechanisms behind this effect by finding that changes in either the nanowire transverse surface orientation,^{51,68} which occur with changes in the nanowire axial orientation, or the nanowire cross-sectional geometry^{54,57} can change the operant modes of plastic deformation. Similarly, Jacobsen et al. found that changes in the quantized conductance of metal nanowires are strongly correlated with the nucleation and propagation of partial dislocations during inelastic deformation.^{67,68}

Thus, both experiments and simulation have shown that despite their significant volume confinement, metal nanowires deform inelastically through traditional dislocation-mediated plasticity. However, a fundamental understanding of how specific nanowire surfaces couple with specific axial orientations with varying geometries to generate predictable deformation modes and nanowire mechanical properties (yield stress, fracture strain, fracture toughness) remains lacking.

Han et al.²⁹ combined TEM and scanning electron microscope (SEM) to study the tensile deformation of sub-100 nm cross-section $\langle 100 \rangle$ silicon nanowires and found that the crystalline silicon lattice became disordered in the necked region prior to failure, indicating the importance of surface effects during the plastic deformation. Interestingly, Menon et al.⁶² documented such crystalline disorder prior to silicon nanowire failure in earlier MD simulations. Furthermore, Han et al.²⁹ observed an increase in ductility with decreasing nanowire size for diameters less than 60 nm at room temperature. In preliminary work, Kang and Cai¹² observed a similar behavior (see Figure 4) from MD simulations and found that while thicker nanowires become ductile only at elevated temperatures, nanowires with diameters less than 4 nm become ductile even at very low temperatures. The discrepancy in the transition diameter between experiments and simulations can be attributed to the much higher strain rate and lack of oxide layer in MD simulations. Nonetheless, the qualitative agreement in the trend between experiments and simulations suggests that the size dependence is a real effect. MD simulations indicate that the mechanism responsible for this transition is that dislocations are more easily nucleated from surfaces of smaller nanowires, while cracks are easier to nucleate from surfaces of larger nanowires.

Recently, Wu et al.⁷² experimentally performed AFM bending of silver nanowires with pre-existing twin boundaries and found that the twin boundaries lead to

strengthening by eliminating favorable slip orientations. This experiment motivated the MD simulations of Cao and Wei,⁵⁹ who found that pre-existing twin boundaries elevate the yield strength of copper nanowires by suppressing dislocation emission and propagation or by forcing dislocations to glide on $\{100\}$ planes after penetrating a twin boundary.⁷³ Afanasyev and Sansoz⁷⁴ also studied the effects of nanoscale twin boundaries during compression of gold nanowires using MD and found that nanowire-free surfaces can deleteriously serve as dislocation escape points; by introducing twin boundaries, they were able to prevent dislocation escape to the free surfaces by inducing slip arrest at the intersection of slip dislocations and the twin boundaries, again resulting in nanowire strengthening.

More recently, Zhang and Huang⁷⁵ found by using MD calculations that twin boundaries do not always lead to nanowire strengthening, and the nanowire surface morphology determines whether twin boundary-mediated nanowire strengthening or softening is observed. Specifically, twin boundaries were found to lower the stress for dislocation nucle-

ation for circular cylindrical nanowires, thus leading to nanowire softening, while an enhanced stress for dislocations to penetrate twin boundaries was found for square cylindrical nanowires, thus leading to nanowire strengthening.

Again, experiments and simulations have demonstrated that nanostructured engineering can be utilized to enhance the strength and post-yield properties of nanowires. Thus, a promising future research direction in nanostructure engineering for nanowires may be in studying interactions of grains with different size and orientation with defects, while paying particular attention to free surface and volume confinement effects.

However, as is well-known, MD simulations of plasticity are conducted at strain rates that are 10–15 orders of magnitude larger than can be obtained experimentally because of computational limitations; this discrepancy is critical because defect nucleation, rather than the motion of existing defects as in bulk metals, is the limiting factor in the ultimate strength of the nanowires. Using novel time scale bridging techniques that are discussed in another article in this issue, Zhu et al.¹⁵ studied the effects of strain rate and temperature on surface-driven dislocation nucleation for compressively loaded copper nanowires. In doing so, they found that the defect nucleation stress under compression is nearly 50% lower at room temperature and strain rates of 10^{-3} s^{-1} as compared to strain rates of 10^8 s^{-1} that are typically found in MD simulations (again due to computational limitations); this demonstrates the importance of time scale bridging simulations as compared to MD in enabling quantitative comparisons between atomistic and experimental results.

Surface-Mediated Nanowire Multifunctionality

Researchers have recently found novel multifunctional properties of both metallic and semiconducting nanowires using atomistic simulations. The initial discovery of this type was made by Diao et al.,^{76,77} who found using MD simulations a surface-stress-driven phase transformation (i.e., without external loading) from $\langle 100 \rangle$ sub-2 nm gold nanowires to a body centered tetragonal (bct) phase, accompanied by nearly 30% compressive strain; it is only at such small nanowire sizes that the surface stresses alone are large enough to cause this phase transformation.

Other metal nanowires that exhibit a surface stress-driven reorientation from $\langle 100 \rangle / \{100\}$ to $\langle 110 \rangle / \{111\}$ were found using MD simulations by multiple

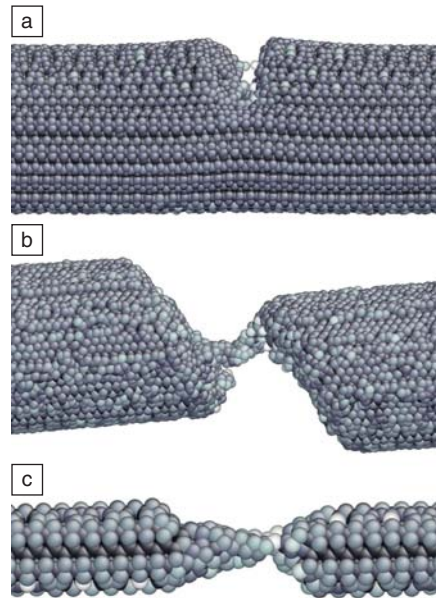


Figure 4. Snapshots of $\langle 110 \rangle$ Si nanowires under tension in molecular dynamics simulations using the modified embedded atom method potential.^{9,12} (a) Brittle fracture of a 7-nm-diameter nanowire at 300 K. (b) Ductile fracture of the same nanowire at 1000 K. (c) Ductile fracture of a 2-nm-diameter nanowire at temperatures as low as 100 K.

researchers. The MD simulations further found that these wires exhibit both novel shape memory and pseudoelastic behavior under tensile loading^{78–82} that is not seen in the corresponding bulk material. The recoverable pseudoelastic strains can reach 40%, which is an order of magnitude larger than bulk shape memory alloys; Park⁷⁹ also found pseudoelasticity in nickel aluminum nanowires. While Kondo and Takayanagi^{83,84} have observed the {100} to {111} surface reorientation that occurs during the predicted nanowire shape memory process in both gold nanowires and gold thin films, the shape memory and pseudoelasticity in metal nanowires has not been observed experimentally due to ongoing difficulties in performing the cyclic thermomechanical loading and unloading of sub-5 nm diameter metal nanowires that are needed to study shape memory-type effects.

Pseudoelasticity also has been found for [0001]-oriented ZnO nanowires using MD simulations. Kulkarni et al.^{85,86} found a novel phase transformation from wurtzite to bct-4 under tensile loading; these results also were obtained using *ab initio* calculations¹³ and MD for nanowire sizes up to 20 nm¹⁰ in diameter as shown in Figure 5a–b. Figure 5a shows the stress-strain response for tensile-loaded ZnO nanowires using MD, where the stress drop indicates that a phase transformation has occurred from wurtzite to bct-4. Figure 5b shows the stresses on atoms in the [2110] plane as the deformation proceeds. Furthermore, all calculations found that surface reconstructions provide the driving force required by these structural transformations.

The pseudoelastic behavior has been reported experimentally for ZnO nanohelices,⁸⁷ which are structurally different than the single crystal ZnO nanowires that were studied using MD. Experimental evidence of the stress-induced phase transformation in ZnO nanowires is not yet available. As shown in Figure 5c–d, recent preliminary *in situ* TEM experiments performed by Agrawal et al.⁴³ instead found brittle fracture along the (0001) cleavage plane at strains approximately equal to the ones needed for the initiation of the phase transformation. It is hypothesized that the absence of the phase transformation in the tested nanowires may either be due to atomic imperfections on the nanowire surface or due to artifacts of the Buckingham potential^{10,39} used in the MD simulations, which accounts for both short-ranged attraction and repulsion, and long-ranged electrostatic interactions. TEM observations show that although the tested nanowires are defect-free in the interior, surface defects in the form of atomic

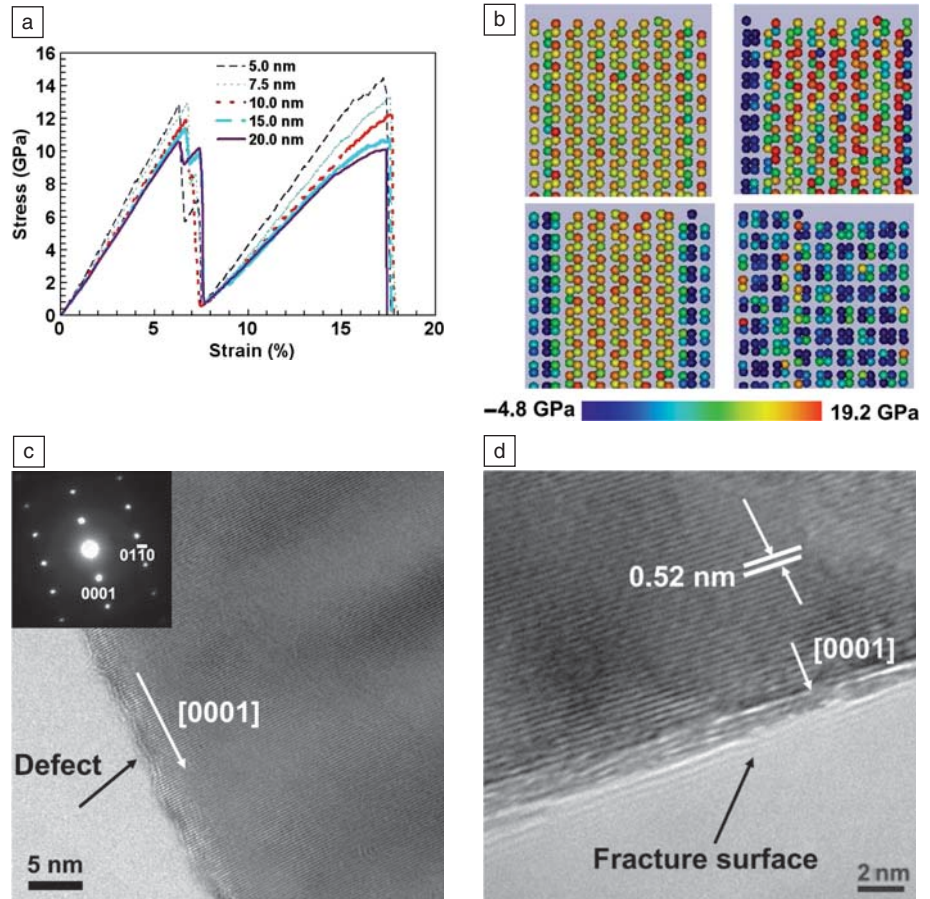


Figure 5. (a) Stress-strain plot of various ZnO nanowire diameters obtained using molecular dynamics. The two drops in stress correspond to a two-step phase transformation from wurtzite to bct-4 (4 here refers to the four-atom rings formed in this configuration). (b) Axial stress plotted for a set of atoms lying in the [2110] plane showing the progression of transformation as strain increases. Note the stress drop in the phase transformed atoms (blue). The strains for the four images are as follows: left top—6.3% (just before the first drop in stress); right top—6.4% (after first drop in stress); left bottom—6.6% (just before the second drop in stress); right bottom—7.5% (after the second drop in stress). (c) Transmission electron microscopy (TEM) image of a nanowire prior to testing showing a single crystal structure in the nanowire interior with some defects on the surface. (d) TEM image of the nanowire after fracture showing the [0001] fracture plane.^{10,43}

roughness are always present. This suggests that such surface imperfections may lead to premature fracture impeding the initiation of the phase transformations.

Conclusions and Future Directions

Atomistic simulations have played an important role not only in developing fundamental insights into the elastic and inelastic behavior and properties of crystalline nanowires, but in predicting new and unexpected properties that may be used to broaden their potential applications. However, reliable design of systems based upon these one-dimensional nanostructures requires resolution of two key issues: (1) discrepancies in the predictions of classical molecular dynamics and

ab initio calculations, particularly when surface reconstructions are involved, and (2) inconsistencies between atomistic predictions and experimental measurements of elastic and inelastic mechanical properties. In this respect, there is a significant need for accurate yet efficient quantum mechanically based multiscale models such that one-to-one comparisons with *in situ* electron microscopy experiments of larger nanowires, while still accounting for surface effects, can be performed; we note that such multiscale models have only recently emerged in the literature.^{88,89} Likewise, progress in experimental approaches that will allow a one-to-one comparison between atomistic simulations and nanoscale measurements is urgently needed.

References

1. C.M. Lieber, Z.L. Wang, *MRS Bull.* **32**, 99 (2007).
2. H.G. Craighead, *Science* **290**, 1532 (2000).
3. C.Q. Sun, B.K. Tay, X.T. Zeng, S. Li, T.P. Chen, J. Zhou, H.L. Bai, E.Y. Jiang, *J. Phys.: Condens. Matter* **14**, 7781 (2002).
4. R.C. Cammarata, *Progr. Surf. Sci.* **46**, 1 (1994).
5. M.E. Gurtin, A. Murdoch, *Arch. Ration. Mech. Anal.* **57**, 291 (1975).
6. J. Wan, Y.L. Fan, D.W. Gong, S.G. Shen, X.Q. Fan, *Modell. Simul. Mater. Sci. Eng.* **7**, 189 (1999).
7. L.G. Zhou, H. Huang, *Appl. Phys. Lett.* **84**, 1940 (2004).
8. H.W. Shim, L.G. Zhou, H. Huang, T.S. Cale, *Appl. Phys. Lett.* **86**, 151912 (2005).
9. K. Kang, W. Cai, *Philos. Mag.* **87**, 2169 (2007).
10. R. Agrawal, B. Peng, E. Gdoutos, H.D. Espinosa, *Nano Lett.* **8**, 3668 (2008).
11. B. Lee, R.E. Rudd, *Phys. Rev. B* **75**, 195328 (2007).
12. K. Kang, W. Cai (2008), submitted.
13. L. Zhang, H. Huang, *Appl. Phys. Lett.* **90**, 023115 (2007).
14. K. Gall, J. Diao, M.L. Dunn, *Nano Lett.* **4**, 2431 (2004).
15. T. Zhu, J. Li, A. Samanta, A. Leach, K. Gall, *Phys. Rev. Lett.* **100**, 025502 (2008).
16. B. Wu, A. Heidelberg, J.J. Boland, *Nat. Mater.* **4**, 525 (2005).
17. A. Heidelberg, L.T. Ngo, B. Wu, M.A. Phillips, S. Sharma, T.I. Kamins, J.E. Sader, J.J. Boland, *Nano Lett.* **6**, 1101 (2006).
18. S. Cuenot, C. Fréty, S. Demoustier-Champagne, B. Nysten, *Phys. Rev. B* **69**, 165410 (2004).
19. G.Y. Jing, H.L. Duan, X.M. Sun, Z.S. Zhang, J. Xu, Y.D. Li, J.X. Wang, D.P. Yu, *Phys. Rev. B* **73**, 235409 (2006).
20. H. Petrova, J. Perez-Juste, Z.Y. Zhang, J. Zhang, T. Kosel, G.V. Hartland, *J. Mater. Chem.* **16**, 3957 (2006).
21. H. Liang, M. Upmanyu, H. Huang, *Phys. Rev. B* **71**, 241403(R) (2005).
22. R. Dingreville, J. Qu, M. Cherkaoui, *J. Mech. Phys. Solids* **53**, 1827 (2005).
23. R.E. Miller, V.B. Shenoy, *Nanotechnology* **11**, 139 (2000).
24. J. Diao, K. Gall, M.L. Dunn, *J. Mech. Phys. Solids* **52**, 1935 (2004).
25. M.T. McDowell, A.M. Leach, K. Gall, *Modell. Simul. Mater. Sci. Eng.* **16**, 045003 (2008).
26. H.S. Park, P.A. Klein, *J. Mech. Phys. Solids* **56**, 3144 (2008).
27. X. Li, T. Ono, Y. Wang, M. Esashi, *Appl. Phys. Lett.* **83**, 3081 (2003).
28. T. Kizuka, Y. Takatani, K. Asaka, R. Yoshizaki, *Phys. Rev. B* **72**, 035333 (2005).
29. X. Han, K. Zheng, Y.F. Zhang, X. Zhang, Z. Zhang, Z.L. Wang, *Adv. Mater.* **19**, 2112 (2007).
30. A.V. Desai, M.A. Haque, *Sens. Actuators, A* **134**, 169 (2007).
31. A.S. Paulo, J. Bokor, R.T. Howe, R. He, P. Yang, D. Gao, C. Carraro, R. Maboudian, *Appl. Phys. Lett.* **87**, 053111 (2005).
32. M. Tabib-Azar, M. Nassirou, R. Wang, S. Sharma, T.I. Kamins, M.S. Islam, R.S. Williams, *Appl. Phys. Lett.* **87**, 113102 (2005).
33. Y. Huang, X. Bai, Y. Zhang, *J. Phys.: Condens. Matter* **18**, L179 (2006).
34. E.W. Wong, P.E. Sheehan, C.M. Lieber, *Science* **277**, 1971 (1997).
35. C.Q. Chen, Y. Shi, Y.S. Zhang, J. Zhu, Y.J. Yan, *Phys. Rev. Lett.* **96**, 075505 (2006).
36. M. Lucas, W. Mai, R. Yang, Z.L. Wang, E. Riedo, *Nano Lett.* **7**, 1314 (2007).
37. X.D. Bai, P.X. Gao, Z.L. Wang, E.G. Wang, *Appl. Phys. Lett.* **82**, 4806 (2003).
38. G. Stan, C.V. Ciobanu, P.M. Parthangal, R.F. Cook, *Nano Lett.* **7**, 3691 (2007).
39. A.J. Kulkarni, M. Zhou, F.J. Ke, *Nanotechnology* **16**, 2749 (2005).
40. J.Q. Broughton, C.A. Meli, P. Vashishta, R.K. Kalia, *Phys. Rev. B* **56**, 611 (1997).
41. G. Cao, X. Chen, *Phys. Rev. B* **76**, 165407 (2007).
42. L. Zhang, H. Huang, *Appl. Phys. Lett.* **89**, 183111 (2006).
43. R. Agrawal, B. Peng, E. Gdoutos, H.D. Espinosa (2008), submitted.
44. Y. Zhu, H.D. Espinosa, *Proc. Nat. Acad. Sci.* **102**, 14503 (2005).
45. Y. Zhu, N. Moldovan, H.D. Espinosa, *Appl. Phys. Lett.* **86**, 013506 (2005).
46. B. Peng, M. Locascio, P. Zapol, S. Li, S.L. Mielke, G.C. Schatz, H.D. Espinosa, *Nat. Nanotechnol.* **3**, 626 (2008).
47. H.S. Park, *J. Appl. Phys.* **103**, 123504 (2008).
48. M. Li, T.S. Mayer, J.A. Sioss, C.D. Keating, R.B. Bhiladvala, *Nano Lett.* **7**, 3281 (2007).
49. H.S. Park, J.A. Zimmerman, *Phys. Rev. B* **72**, 054106 (2005).
50. J. Diao, K. Gall, M.L. Dunn, *Nano Lett.* **4**, 1863 (2004).
51. H.S. Park, K. Gall, J.A. Zimmerman, *J. Mech. Phys. Solids* **54**, 1862 (2006).
52. J. Monk, D. Farkas, *Philos. Mag.* **87**, 2233 (2007).
53. H. Mehrez, S. Ciraci, *Phys. Rev. B* **56**, 12632 (1997).
54. A.M. Leach, M. McDowell, K. Gall, *Adv. Funct. Mater.* **17**, 43 (2007).
55. Z. Wang, X. Zu, L. Yang, F. Gao, W.J. Weber, *Phys. Rev. B* **76**, 045310 (2007).
56. A.S.J. Koh, H.P. Lee, *Nano Lett.* **6**, 2260 (2006).
57. C. Ji, H.S. Park, *Appl. Phys. Lett.* **89**, 181916 (2006).
58. B. Hyde, H.D. Espinosa, D. Farkas, *JOM* **57**, 62 (2005).
59. A. Cao, Y. Wei, *Phys. Rev. B* **74**, 214108 (2006).
60. Y.-C. Lin, D.-J. Pen, *Nanotechnology* **18**, 395705 (2007).
61. P.Z. Coura, S.G. Legoas, A.S. Moreira, F. Sato, V. Rodrigues, S.O. Dantas, D. Ugarte, D.S. Galvao, *Nano Lett.* **4**, 1187 (2004).
62. M. Menon, D. Srivastava, I. Ponomareva, L.A. Chernozatonskii, *Phys. Rev. B* **70**, 125313 (2004).
63. N. Agrait, G. Rubio, S. Vieira, *Phys. Rev. Lett.* **74**, 3995 (1995).
64. E.Z. da Silva, A.J.R. da Silva, A. Fazzio, *Phys. Rev. Lett.* **87**, 256102 (2001).
65. U. Landman, W.D. Luedtke, B.E. Salisbury, R.L. Whetten, *Phys. Rev. Lett.* **77**, 1362 (1996).
66. W. Liang, M. Zhou, *Proc. Inst. Mech. Eng., C: J. Mech. Eng. Sci.* **218**, 599 (2004).
67. M. Brandbyge, J. Schiøtz, M.R. Sørensen, P. Stoltze, K.W. Jacobsen, J.K. Nørskov, L. Olesen, E. Laegsgaard, I. Stensgaard, F. Besenbacher, *Phys. Rev. B* **52**, 8499 (1995).
68. M.R. Sørensen, M. Brandbyge, K.W. Jacobsen, *Phys. Rev. B* **57**, 3283 (1998).
69. J. Diao, K. Gall, M.L. Dunn, J.A. Zimmerman, *Acta Mater.* **54**, 643 (2006).
70. P.E. Marszalek, W.J. Greenleaf, H. Li, A.F. Oberhauser, J.M. Fernandez, *Proc. Nat. Acad. Sci.* **97**, 6282 (2000).
71. V. Rodrigues, T. Fuhrer, D. Ugarte, *Phys. Rev. Lett.* **85**, 4124 (2000).
72. B. Wu, A. Heidelberg, J.J. Boland, J.E. Sader, X. Sun, Y. Li, *Nano Lett.* **6**, 468 (2006).
73. J. Wang, H. Huang, *Appl. Phys. Lett.* **88**, 203112 (2006).
74. K.A. Afanasyev, F. Sansoz, *Nano Lett.* **7**, 2056 (2007).
75. Y. Zhang, H. Huang, *Nanoscale Res. Lett.* **4**, 34 (2009).
76. J. Diao, K. Gall, M.L. Dunn, *Nat. Mater.* **2**, 656 (2003).
77. J. Diao, K. Gall, M.L. Dunn, *Phys. Rev. B* **70**, 075413 (2004).
78. W. Liang, M. Zhou, F. Ke, *Nano Lett.* **5**, 2039 (2005).
79. H.S. Park, *Nano Lett.* **6**, 958 (2006).
80. W. Liang, M. Zhou, *J. Eng. Mater. Technol.* **127**, 423 (2005).
81. W. Liang, M. Zhou, *Phys. Rev. B* **73**, 115409 (2006).
82. H.S. Park, C. Ji, *Acta Mater.* **54**, 2645 (2006).
83. Y. Kondo, K. Takayanagi, *Phys. Rev. Lett.* **79**, 3455 (1997).
84. Y. Kondo, Q. Ru, K. Takayanagi, *Phys. Rev. Lett.* **82**, 751 (1999).
85. A.J. Kulkarni, M. Zhou, K. Sarasamak, S. Limpijumnong, *Phys. Rev. Lett.* **97**, 105502 (2006).
86. J. Wang, A.J. Kulkarni, K. Sarasamak, S. Limpijumnong, F.J. Ke, M. Zhou, *Phys. Rev. B* **76**, 172103 (2007).
87. P.X. Gao, W. Mai, Z.L. Wang, *Nano Lett.* **6**, 2536 (2006).
88. V. Gavini, K. Bhattacharya, M. Ortiz, *J. Mech. Phys. Solids* **55**, 697 (2006).
89. M. Fago, R.L. Hayes, E.A. Carter, M. Ortiz, *Phys. Rev. B* **70**, 100102(R) (2004). □



www.mrs.org/mymrs

This feature of the MRS Web site allows you to personalize the information you receive from us—identify your particular areas of interest, register for/manage your online newsletters and alerts, change your password, and update your contact information.

May 31- June 12, 2009

LEHIGH MICROSCOPY SCHOOL

Lehigh University, Bethlehem, PA, USA

MAIN COURSES

SCANNING ELECTRON MICROSCOPY
AND X-RAY MICROANALYSIS

June 1-5

INTRODUCTION TO SEM AND EDS
FOR THE NEW OPERATOR

May 31

ADVANCED COURSES

SCANNING PROBE MICROSCOPY:
From Fundamentals to
Advanced Applications

June 8-11

PROBLEM SOLVING WITH SEM,
X-RAY MICROANALYSIS,
AND ELECTRON
BACKSCATTER PATTERNS

June 8-12

QUANTITATIVE X-RAY
MICROANALYSIS:
Problem Solving using EDS
and WDS Techniques

June 8-12

SCANNING TRANSMISSION
ELECTRON MICROSCOPY:
From Fundamentals to
Advanced Applications

June 8-11

FOCUSED ION BEAM (FIB):
Instrumentation and Applications

June 8-11

For more information, contact:

Sharon Coe | 610.758.5133 | sharon.coe@lehigh.edu

www.lehigh.edu/microscopy

39 YEARS OF EXCELLENCE